designs

MDPI

Article

Grid generation for CFD analysis and design of a variety of twin screw machines

Sham Rane [1,2,*], Ahmed Kovačević [1] and Nikola Stošić [1]

[1] Centre for Compressor Technology, City, University of London, EC1V 0HB, UK;
[2] Department of Engineering Science, University of Oxford, OX2 0ES, UK;
* Correspondence: sham.rane@eng.ox.ac.uk

Received: date; Accepted: date; Published: date

Abstract: Detailed analysis of flow and thermodynamics in positive displacement screw machines demands for 3D CFD modelling. The advantage of such simulations is that the model, including leakage gaps, captures real geometry of the rotors and the ports. However, exploration of non-conventional designs of rotary machines has been significantly constrained by availability of their computational grid, used for CFD. SCORG is a customized grid generation tool that has a framework developed for classical twin screw machines. In this research, application of this tool has been extended to other variety of screw machines such as variable geometry rotors with lead or profile variation. Similarly, a completely non-conventional internally geared conical screw machine could be designed. Other arrangements include multiple gate rotors intended to increase volumetric displacement or the dual lead, high wrap angle rotors intended for very high-pressure differences and vacuum applications. The availability of a computational grid for such screw rotors now makes it possible to evaluate the flow and thermal field in the working chambers of these machines. A water injected twin screw compressor case study has been presented to demonstrate use of the developed grid generation tools in analysis and design.

Keywords: rotary screw machines; CFD; grid generation; screw compressor; screw expander; screw pump; variable geometry rotor

1. Introduction

Today screw machines are regarded as highly reliable and compact systems for energy conversion. The twin screw and single screw compressors are the most widely used types of industrial compressors. Figure 1 presents the geometry of a pair of a twin screw compressor. Opening of the space between the rotor lobes to the suction port fills the gas into the passages formed between them and the casing, until the trapped volume is a maximum. Further rotation leads to cut off the chamber from the suction port and progressive reduction in the trapped volume thus compressing the gas. This also leads to axial and bending forces on the rotors and to contact forces between the rotor lobes. The compression process continues until the required pressure is reached when the rear ends of the passages are exposed to the discharge port through which the gas flows out of the compression chamber at approximately constant pressure. Apart from these conventional designs, there are some variants described in literature and under research. Continuing demands for reduced energy losses and higher gas pressure differences in compact machines have led to the use of modern analytical tools to predict the flow characteristics and performance of non-conventional types of screw machines, such as those with rotors of variable geometry. Figure 2 presents possibilities of variable geometry screw machines [1]. These non-conventional screw machines are based on the same operating principles but there are differences in the rotor geometry, the number of rotors or the rotor mutual orientations. Thereby, these non-conventional machines can obtain improvements in performance and design benefits.

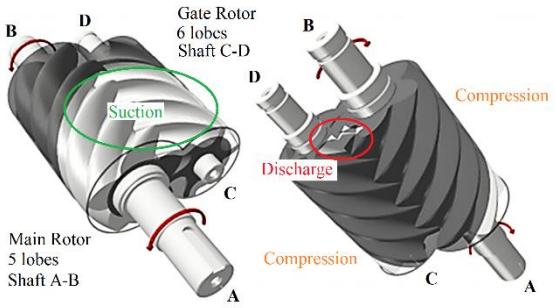

Figure 1. Conventional twin screw rotors with N 5-6 profile

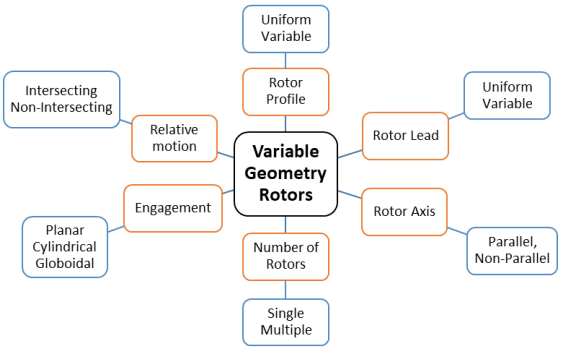

Figure 2. A representation of possibilities for rotary screw machine geometries [1]

There is a lack of 3D computational methods available for design and analysis of such screw machines. Screw compressor rotors with a variable lead are still at the research stage, although a patent on this concept dates back to 1969 [2]. This describes a helical screw compressor with a continuously variable lead for the lobes of the male and gate rotors. Figure 3a shows the meshing of twin screw rotors with variable helical lead. It has been shown that for the same rotor lengths, diameter, wrap angles and lobe profiles the variable pitch rotors can be designed to provide higher pressure ratios and larger discharge port opening areas, thus reducing the exit throttling losses [2]. Advantages of variable pitch rotors, can also be comprehended if the rotor diameters are made to vary from suction to the discharge. Figure 3b shows an example of a parallel axis variable profile twin screw rotors. As the rotors of a screw machine turn during operation, the fluid volume in between them is deformed (compressed or expanded) and the CFD grid which represents the fluid volume also needs to deform. Without capturing this deformation it is not possible to capture the real three dimensional fluid characteristics inside the working chamber. A breakthrough was achieved in 1999 by Kovačević et al. [3, 4] with the use of an analytical rack generation method, proposed by Stošić [5], applied to generate an algebraic, adaptive, block structured, deforming grid calculation for twin screw rotors. This methodology of deforming grid generation was implemented in the customized grid generation tool called SCORG [1, 3, 4, 6].

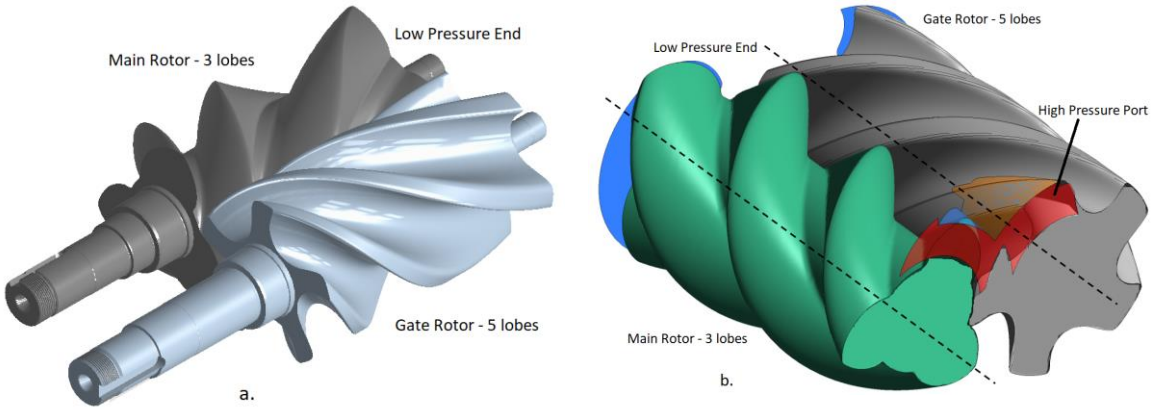

Figure 3. Non-conventional variable geometry twin screw rotors with N 3-5 profile. a) Variable lead b) Variable rotor profile [1, 18]

Since then there have been several studies reported on the CFD analysis of twin screw machines. The use of this method for screw compressor applications is justified by its ease of use and its speed. The analysis of the working chamber is transient in nature and requires a grid representing every time step rotor position and domain deformation (ALE solver formulation, [1]). In this respect, algebraic methods can be used to recalculate the grid quickly. SCORG has been written in FORTRAN with a C# front end application [6]. In his thesis, Kovačević [3] presented the grid generation aspects in detail. Several CFD simulations of twin screw machines to predict flow, heat transfer, fluid-

structure interaction, etc have been reported in [3, 4, 6]. Sauls and Branch [7] used the results from CFD calculations to develop an improved one-dimensional thermodynamic model for refrigerant screw compressors, by extracting calibration coefficients that influence the pressure variation during the discharge process. Mujić [8] presented an optimisation of the discharge port area based on flow behaviour in the discharge chamber. CFD model was used for relative comparison of port geometry modifications and their influence on predicted pressure pulsations has been used to judge sound spectrum and noise level from the compressor. These noise levels predicted by CFD solutions have been used for designing discharge ports with reduced noise levels. Mujić [8] in his thesis presented a 3D CFD coupled model in which the boundary conditions for the discharge port were obtained as time varying data from 1D thermodynamic chamber models. The procedure was implemented for Star CCM+ solver. It was found that the results predicted by the coupled model for sound pressure levels were closer to the full 3D CFD models and also in close agreement with the experimental measurements. Such an approach simplified the numerical analysis and also provided faster results from the CFD models. Vierendeels et al. [9] were the first to implement a grid generation algorithm for block structured mesh from the solution of the Laplace equation for twin screw compressors and pumps using differential methods. The use of differential methods requires the PDE to be solved for every rotor position and then the grid generation has to be repeated from the equipotential and gradient lines. In his thesis, Vande Voorde [10] presented the principles of solving the initial Laplace equation and then using it to construct a block structured deforming mesh. Based on this grid generation, flow in a double tooth compressor and a twin screw compressor was analysed and the results were compared with experimental data over a range of discharge pressures and rotor speeds. A detailed comparison of the algebraic and differential methods has been presented by Rane and Kovačević [1, 11]. In [12] these techniques implemented in SCORG have been validated for a dry air twin screw compressor at various operating conditions and with various type of computational grids.

In case of non-conventional screw machines, recently, Schulze-Beckinghausen et al. [13] have presented a thermodynamic chamber model and compared the results of the variable lead compressor performance with constant lead rotors. Their model predicted higher compression with rotors of varying pitch. The volumetric efficiency showed an improvement compared to constant lead rotors but the indicated power was high due to non-optimal internal pressure rise, which increased the specific power. Utri and Brümmer [14] presented a thermodynamic comparison of screw expanders with constant and variable pitch in an ORC system. Instead of a continuous lead variation, they considered a stepped variation which gives a larger port area for the high pressure filling part of the cycle. The overall wrap angle on the rotors was maintained equal to 245°. A multi chamber thermodynamic model was then used to evaluate and compare the performance of different configurations. Rotors with variable rotor pitch showed an increase of up to 5% in effective power output. Kauder and Fost [15] and Fost [16] evaluated options to modify screw rotors to improve the filling process in screw expanders and proposed a few non-conventional concepts like conical rotors and rotors with inlet discs, each with a different pitch. Conical rotors had a variable rotor profile, similar to rotors in Figure 3b, and showed an improvement in chamber filling mainly influenced by a reduction in pressure loss at the inlet. For the same built in volume index V_i = 5, the max inlet area showed an increase from 540mm^2 to 1080mm^2. All these studies were done with the intention of predicting the performance and characteristics of screw machines at the design stage and optimizing the geometry and control parameters for a given application and operating condition. With vast improvements in computational technology and availability of more accurate calculation methods, the use of Computational Fluid Dynamics for screw machine design has been encouraged as it would provide better insight into the flow dynamics within them. CFD model of such non-conventional variable geometry was studied by the authors in [1, 17, 18]. In this paper, recent advancements of implementation of differential grid [19] using a PDE solution of the Poisson's form in SCORG grid generator has been presented. The quality of numerical cells and their distribution obtained by this differential method is greatly improved making the grid suitable for multiphase models such as oil injected screw compressors [21, 22, Video S2]. A special procedure has been introduced that completely smooths the transition of the partitioning rack curve between the two rotors thus

improving grid node movement and robustness of the CFD solver [20]. Further, application of SCORG tool to a variety of screw machines such as variable geometry rotors with lead or profile variation, internally geared conical screw machine, multiple gate rotors and dual lead, high wrap angle rotors are shown. Case study of a water injected twin screw compressor [24] has been presented to demonstrate use of the developed grid generation tools in analysis and design.

2. SCORG – customized rotor CFD grid generation

An analytical grid generation of screw machine working domain is explained in Kovačević et.al [3, 4]. It includes separating domains of the screw rotors by a rack curve [5] and forming independent flow domains around each of the rotors. After the grid points are distributed on boundaries, an initial grid is obtained by TFI. Recently, in order to achieve a conformal single domain mesh, Rane and Kovacevic [11, 12] introduced a new approach of background blocking. In this procedure, the outer boundary in each background block (Figure 4a), a coarse analytically generated mesh, is defined as a combination of the rack segment and the casing circle segment. The rack segment stretches between the bottom and top cusp points and is closed by the casing. The distribution obtained on the outer boundaries of the two blocks is used to constrain distribution on rotor profile as shown in Figure 4a.

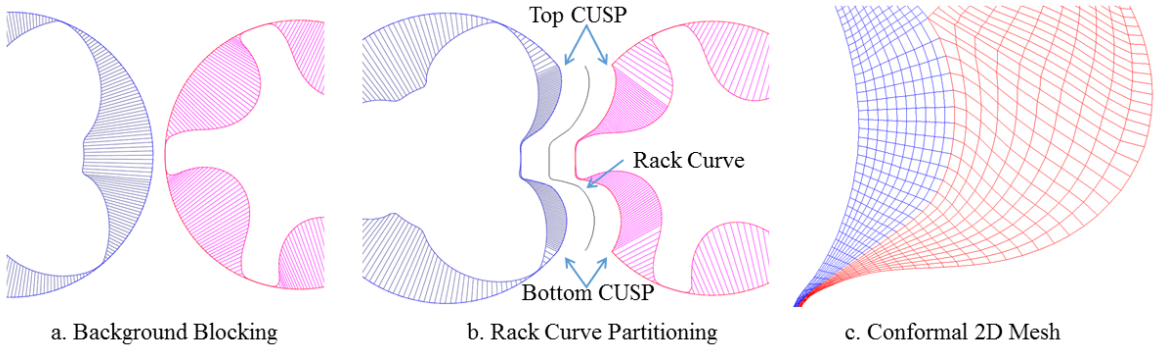

Figure 4. Background blocking used in SCORG for differential mesh

Figure 4b shows how the rack curve is used to partition the two rotor domains and the boundary distribution so obtained is used to generate the 2D mesh using TFI. Using the blocking approach allows both conformal and non-conformal boundary map to produce fully hexahedral 3D grid. Figure 4c shows the nodes on the rack segment between the main and the gate rotor grids with conformal boundary map. The 3D mesh generated from such 2D cross sections allows the rotor domains of the male and female rotors to be combined into a single rotor mesh. This avoids inaccuracies and instabilities that may arise due to the interface mismatch in a non-conformal boundary map. The resultant grids are recommended for oil injected multiphase flow modelling and have been described in more detail by Rane and Kovacevic in [20, 22, Video S2]. However, even with this approach, during the operation as the rotors rotate, the rack curve comes to a position when it transitions with a relatively large deformation between the two consecutive steps. The lone algebraic method results in this transition as a step change at certain positions as shown in Figure 6b and 6c. One of the objectives of the elliptic PDE mesh generation implemented in SCORG was to improve the time transition of the partitioning rack curve between the two rotor domains.

Techniques based on solutions of Partial Differential Equations (PDE) to define coordinate transformation are widely used in grid generation. The idea of using elliptic PDE like Laplace equation or Poisson equation is based on the work of Crowley and Winslow, and it is in detail described in Knupp and Steinberg [19]. Elliptic PDE's have certain beneficial properties in their solution that make them preferable for body fitted curvilinear grids. These are less prone to folding of mesh lines, introduce inherent smoothness so that the discontinuities over the boundaries are not propagated into the interior of the domains and the physical boundaries can be exactly used as boundary conditions in the computational space. But the numerical grid generation is computationally expensive without an initial grid. If an initial grid based on algebraic method could be used, the required time for the solution of PDE's is significantly reduced. This treatment requires

the solution of the coupled PDE equations in which schemes like Tri-diagonal Matrix Algorithm can be used for the solution [19]. The boundary conditions are specified as grid coordinates at computational boundaries. This means that for the generation of grid in twin screw rotor domain the coordinates of the boundary nodes need to be used as boundary condition. At this stage the initial grid generated by the TFI is used for both initial condition and boundary conditions. An O grid topology produced by TFI shown in Figure 5b has been used by the differential solver with successive-over-relaxation procedures as described in Knupp and Steinberg [19]. In addition, the convenient input parameters are used to control intensity of smoothing and inflation layer formation of the elliptic solver. The final O grids generated separately for the two rotors by the differential solver are merged to produce a single domain mesh for the two rotors as shown in Figure 5d. The PDE solver is also used in the interlobe area bounded by the cusp radial nodes (Figure 4b) to convert the rack curve into a smooth transitioning curve across the specified number of angular positions of the rotor. This is obtained over a four step procedure to gradually change the partition between the two O grids into a smooth one as shown in Figure 5a to 5d.

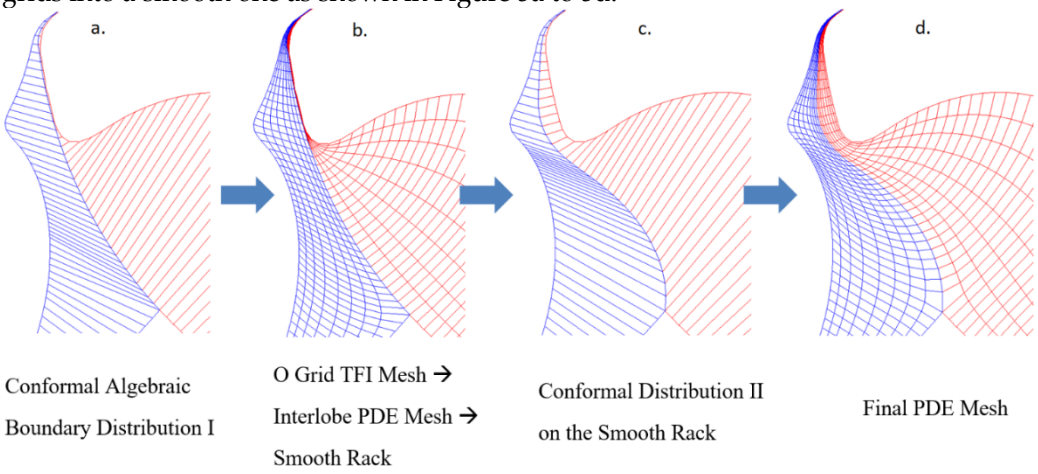

Figure 5. Four-step procedure for improving time transition of the rack curve

The smooth rack obtained by this procedure is supplied back to a second stage of boundary distribution calculation resulting in a new conformal distribution. This conformal distribution is further used as a boundary condition for final differential mesh generation. As a result a significant improvement in the mesh quality is achieved. Figure 6 shows the comparison of the cell orthogonal quality between the algebraic meshes and the elliptic meshes. Figure 6(a-d) are algebraic meshes and Figure 6(e-h) are elliptic meshes in the respective rotor positions.

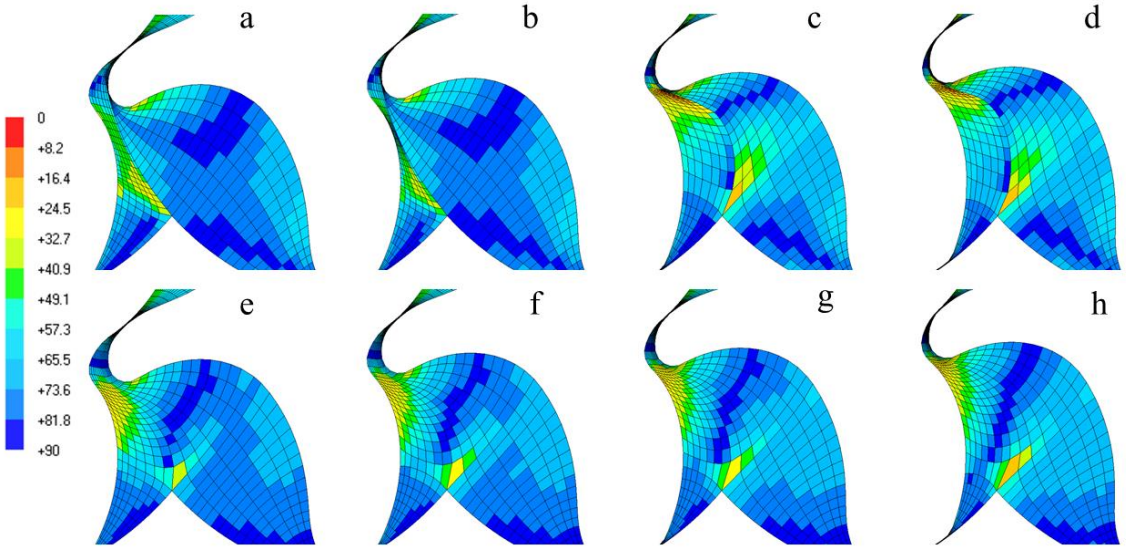

Figure 6. Comparison of cell orthogonal quality between Algebraic (a-d) and Elliptic (e-f) meshing

The values for the minimum orthogonal angle of the algebraic meshes (top) drops to about 8 degree after the rack curve transitions from position b to c. The majority of cells are in the range of 40 – 60 degree orthogonality. Low orthogonality values are also noticed in the position d. But in case of elliptic meshing, the overall orthogonality has greatly improved so that the minimum orthogonal angle is 25 degree. Most of the cells are in the range of 75 – 90 degree orthogonality. There is one cell at the bottom cusp which shows low orthogonality of about 15 degree in both sets of meshes which is the consequence of the discontinuity at cusp point and it cannot be avoided. However the overall mesh quality is greatly improved. With these techniques a good quality quadrilateral cell structure can be constructed in the 2D cross sections of the rotor. Data from 2D cross sections is then combined together to construct the full 3D grid representing the main and gate rotor position and a set of such 3D grids need to be generated with successive increments in the rotor position and provided to the flow solver during numerical analysis [1].

2.1. Conventional twin screw machine

Figure 7 shows the computational grid of a conventional twin screw machine. This example is that of a water injected twin screw compressor [24]. The case study analysis is presented in section 3. SCORG generates a set of 2D cross-sections with quadrilateral cells as seen in one rotor profile position in Figure 7. These set of 2D sections are then assembled as 3D rotor domain grids as seen in Figure 7 for one rotor position. Several such rotor position 3D node positions data are produce by SCORG and supplied to the flow solver during computations. A priori generation of 3D grid data for all the cyclically repeating rotor positions ensures that the solver will function robustly (without failing due to cell degeneration) during the simulation.

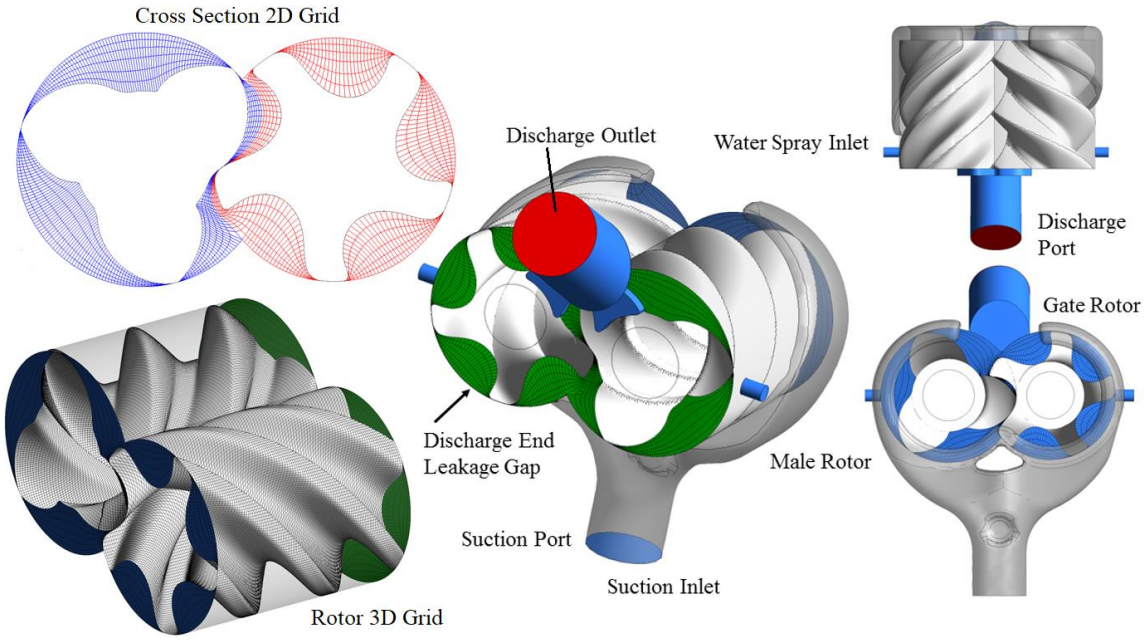

Figure 7. Flow domain and rotor grid of a water injected twin screw compressor [24]

A choice of hexahedral structure allows for ease of database and at the same time ALE formulations in the solver can be utilised that only demand for accurate node positions with time in order to capture grid deformation. Decomposition of the working chamber consists of splitting the flow region into three main blocks as shown in Figure 7. This gives the flexibility to treat mesh generation in these blocks independently, on the choice of the grid generation methods. In a single domain mesh both the rotors are contained in one deforming grid block thereby eliminating the non-conformal interface between the rotors. The deforming rotor grid has non-conformal interfaces with static ports and the water injection port.

2.2. Variable lead twin screw machine

Figure 3a shows the meshing of twin screw rotors with variable helix lead. SCORG can be used to generate the deforming rotor domain grid for such variable lead rotors [1, 18]. A pitch variation function is specified for the rotors and used to derive a relation between the fixed angular increments of from one section to the other and the required variable axial displacements (Δz), for each cross section of the rotor. So the grid vertex data generated for one interlobe are reused but positioned in the axial direction with variable Δz, such that the pitch variation function gets applied. An example rotor and the pitch function is shown in Figure 8 where suction side pitch was 130mm and discharge side pitch was 40mm.

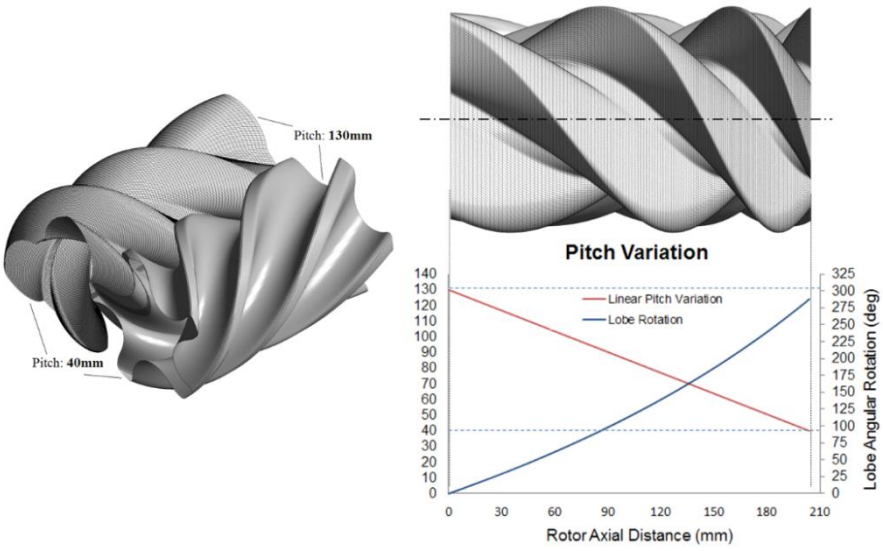

Figure 8. Variable lead screw rotor grid with 3/5 'N' profile [1, 18, Video S1]

In [1], a comparative study has been presented between uniform pitch (85mm) with built in volume index V_i of 1.8 and 2.2, and variable pitch (Figure 8) with V_i > 1.8. The wrap angle of 285° was maintained as shown in Figure 8 for both the rotors. The analysis showed that by varying the rotor lead continuously from the suction to the discharge ends, it is possible to achieve steeper internal pressure build up. Varying the rotor lead also allows a larger discharge port area, thereby reducing throttling losses, and increase in volumetric efficiency (η_v) by reducing the sealing line length in the high pressure zone. Uniform rotors show highest volumetric efficiency at 2.0 bar. But with V_i = 2.2 the efficiency was lower than that of the variable pitch rotors due to comparable internal pressure rise and comparatively shorter sealing line length. An improvement in η_v of 2.2% at 2.0 bar and 2.0% at 3.0 bar discharge pressure was reported for the variable lead rotor.

2.3. Variable profile twin screw machine

The SCORG grid generation algorithm has been extended to variable profile rotors in [1]. The functionality also allows a covariation of rotor lead as well as rotor profile. An example of uniform lead and variable profile rotor is Figure 3b and the grid generated by SCORG is shown in Figure 9. In this algorithm, the additional computational effort required is to calculate the 2D grid data in every cross section as compared to that of a uniform pitch rotor grid generation calculation. The assembly of the grid from 2D to 3D structure was completely redesigned in order to provide flexibility to generate grids for variable geometry rotors. The inputs for the geometry of the rotor can be provided as a set of profile coordinate files for the main and gate rotors in each cross section. These data points can be extracted from CAD models. In the case of profiles such as the 'N' profile which are defined by a generating rack, a set of rack coordinate files for each of the rotor cross section could be used. A comparative study between uniform profile and variable profile rotors has been presented in [1]. In case of the variable profile, addendum on the suction end of the rotors was 33mm while on the

discharge side it was reduced to 21mm. The addendum on the uniform profile rotors had constant value 28.848mm. Due to the variation of addendum the outer diameter of the male rotor changes while the inner diameter remains constant and vice versa for the female rotor, as shown in Figure 9. The volumetric displacement of these rotors was smaller than that of the uniform profile rotors. Analysis of variable profile rotors showed a steeper internal pressure rise but there was no reduction of the sealing line length and blow-hole area for the same size of the rotors. The increase in root diameter of the female rotors with variable profile certainly helps in producing stiffer rotors for high pressure applications. There was not much gain in η_v with variable profile rotor at 3.0bar due to there being no significant reduction in the sealing line length.

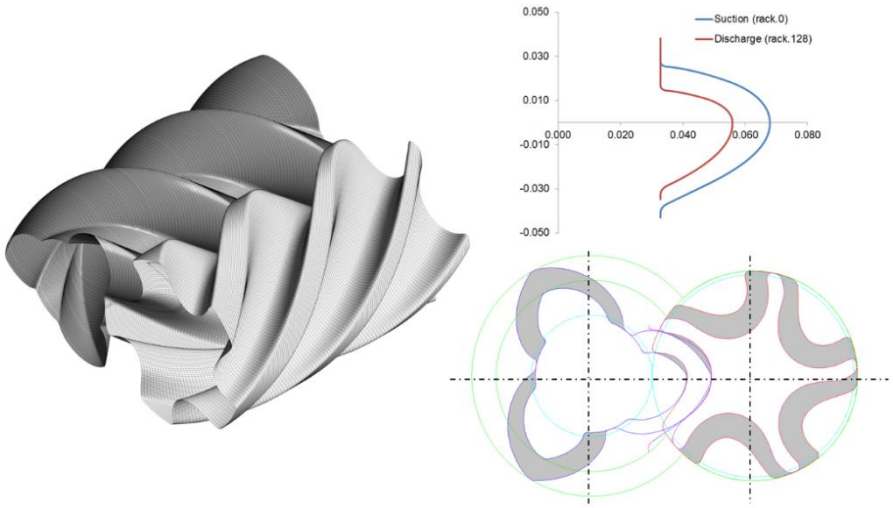

Figure 9. Variable profile screw rotor grid with 3/5 'N' profile [1, 18]

A 1.2% reduction in η_v was observed at 2.0 bar due to smaller capacity of the machine and higher internal pressure rise with over-compression. The uniform rotors show the highest adiabatic efficiency (η_a) at 2.0 bar. However, with V_i = 2.2 their η_a was lower than that of the variable geometry rotors. At 3.0 bar, the uniform rotors have reduced adiabatic efficiency (still 0.7% higher than variable geometry rotors) but both variable pitch and variable profile rotors show an increment in adiabatic efficiency due to a balanced internal pressure rise. An improvement of 2.8% at 2.0 bar and 1.0% at 3.0 bar with variable lead and 1.1% at both pressures with variable profile was reported.

2.4. Tri rotor screw machine

As the pressure difference between suction and discharge increases in screw compressors, the rotor root diameter has to increase, in order to be able to endure bending loads and avoid rotor damage. Also, the number of rotor lobes has to be increased. Consequently, there is a decrease in the volumetric displacement achieved by a given size of the machine. One of the methods of achieving higher volumetric displacement is by running two or more compressors in parallel. Another approach is to utilize a single male rotor and multiple female rotors to effectively increase the number of compression chambers and boost the flow rate. One arrangement for two female rotors is shown in Figure 10, which is similar to the patent by Nilsson [23]. The suction and discharge in this configuration happen on both axial ends of the male rotor and this can help in reducing the radial load on it. The design of the ports is challenging because the end plates have to accommodate heavy bearings. This increases the chances of having the full pressure difference across a leakage path, increasing the effective leakage as compared to twin screw arrangement. Such a possibility and also the port design can be investigated further in detail by CFD analysis and the required multi-gate rotor grid can be generated using SCORG.

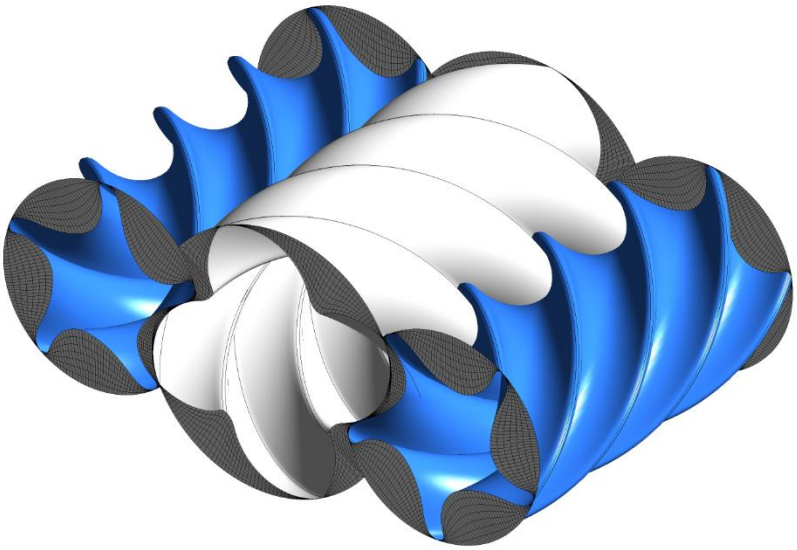

Figure 10. Tri rotor screw compressor grid with 4/5 'N' profile [Video S3]

2.5. Internally geared twin screw machine

Another example of grid generation with uniform pitch and variable section is the design of internally geared twin screw machine. A 3/4 lobe combination compressor with cycloidal profiles can be generated using SCORG as shown in Figure 11. The rotor diameter changes along the length with the helical spiral of a constant pitch. In comparison to a classical twin screw compressor, there are two screw rotors but the gate rotor is an internally lobed helical spiral rotor driven by the inner main screw rotor which is externally lobed. The compression chamber is formed in the volume trapped between the inner and the outer rotors. The reduction of volume occurs because of the progressive reduction of the rotor diameter due to scaling of the profile along the spiral. This in turn causes internal compression and increase in pressure. In operation, the outer rotor is positioned on a central axis while the inner rotor rotates about an eccentric axis with varying centre distance from the suction to the discharge ends. Both axes are stationary in space.

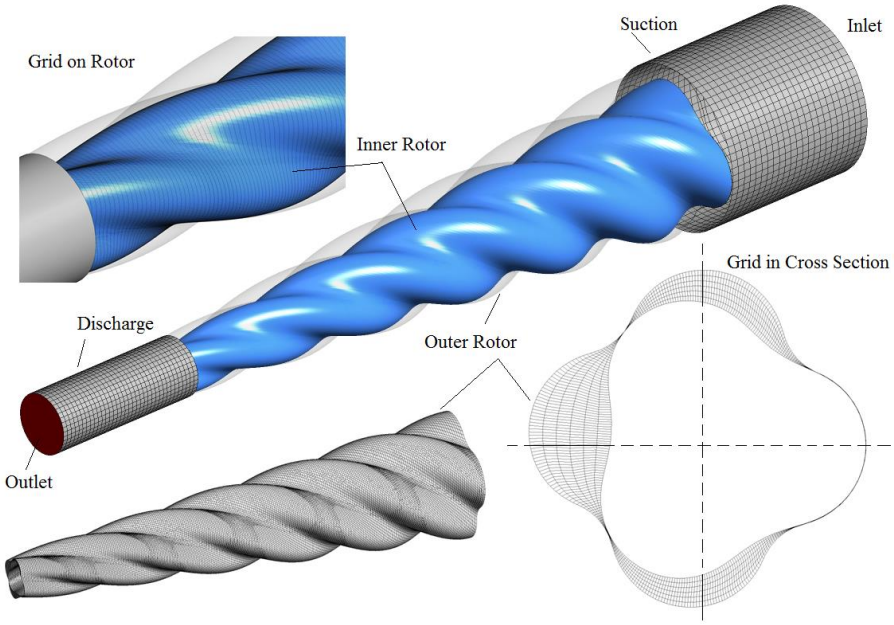

Figure 11. Grid of the working chamber of conical internally geared screw rotors [1, Video S4]

2.6. Dual lead twin screw machine

In liquid pumping application with very high pressure difference between suction and discharge or in vacuum pumps the conventional screw rotor has a very high wrap angle in the order of 1080º.

316 In comparison, a twin screw compressor has a wrap angle in the range of 250 – 310º. The large wrap
317 angle severely reduces the volumetric capacity of such pump rotors. One of the means of increasing
318 displacement is to use a dual lead rotor as shown in Figure 12. SCORG can generate rotor grid for
319 such high wrap angle rotors and can construct dual/multiple lead sections.
320

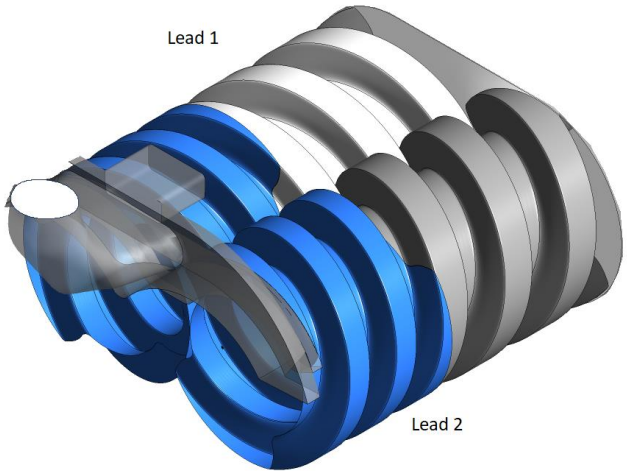

321
322 **Figure 12.** Grid of the working chamber of dual lead, high wrap angle, screw pump rotors

323 **3. Application of SCORG grid for analysis of water injected twin screw compressor**

324 There are industrial processes requiring clean compressed air where oil contamination is not
325 acceptable such as in the food and pharmacy plants. In the absence of oil in the compression chamber,
326 leakage and thermal deformation causes significant limitation on the delivery pressures that could
327 be achieved in one compression stage. As such multistage compression with intercooling has been
328 employed which adds immensely to the cost of the compressor plant. Injection of liquid water in twin
329 screw air compressors has been pursued for long due to the thermodynamic benefits that supersede
330 a dry air compression process. When water is used in small quantities during the compression
331 process an internal cooling and sealing can be achieved and also a condenser fitted downstream of
332 the compressor can strain the water out of delivered high pressure air. In such a system or when there
333 are no condensers employed it is desirable to inject an optimum quantity of water into the
334 compression chamber to gain evaporative cooling. Recent studies have shown that using CFD models
335 for dry air and oil injected air compressors achieved a good agreement with measurements, in
336 prediction of performance parameters [22]. In these simulations, the Eulerian-Eulerian multiphase
337 modelling has been applied. To implement the same model for water injected compressors presents
338 an additional challenge that the liquid water injected into the compression chamber changes phase
339 and evaporates depending on local saturation and thermodynamic conditions [24]. Water also forms
340 liquid film on the rotor and housing and thereby influences thermal changes. The objective of the
341 present analysis was to estimate the temperature distribution inside the compressor, identify non-
342 uniformity and provide data to estimate thermal deformations due to high temperatures. CFD model
343 was used to calculate four different operating conditions with gradually increasing water content.
344 The analysis indicates that with an increased amount of water injection into the compression chamber
345 it is possible to control the gas discharge temperature in the limits of 200°C for the safe operation of
346 selected bearing and seals.

347 *3.1. CFD model and operating conditions*

348 Description of typical CFD modelling for twin screw compressors in presented in detail in Rane
349 [1, 11, 12]. The whole working domain of the compressor is split into four main sub-domains namely
350 rotor domain, suction port, discharge end leakage gap and discharge port. All sub-domains are
351 connected in the solver by non-conformal interfaces. The grid for the rotor domain is generated using
352 SCORG while grids for all stationary domains are obtained using ANSYS meshing. ANSYS CFX

solver is used in this study. An inhomogeneous formulation treats momentum transport for each phase separately and can account for high slip conditions. Evaporation of water-liquid phase is defined as per equation (1) and the saturation temperature $T_{sat,\hat{p}} = 184.06℃$ is specified with latent heat $L = 1998.55$ kJ/kg in equation (2) corresponding to 11.0 bar delivery pressure. An empirical form of the Lee model [24] has been used in the present study. It is assumed that during the entire compression process from suction pressure to discharge pressure, secondary phase water-liquid changes phase to water-vapour only when its temperature T_w exceeds the saturation temperature at discharge pressure T_{sat,p_d}. Such high temperatures can occur inside the compression chamber due to the heat addition of compression and reheating of leakage gas. A possible internal over-compression is another contributor. Another crude assumption is that the phase change is unidirectional i.e. only evaporation occurs and no condensation. It is anticipated that condensation if it has to occur will happen in the discharge pipes and not in the compression chamber where continuous heat addition occurs. As discharge piping is not a part of the computational domain, condensation can be ignored. Once the water-liquid is evaporated it is artificially removed from the domain. The entire enthalpy of evaporation is extracted from the primary phase air resulting into cooling. In empirical form the evaporation mass transfer rate for water-liquid phase is

If $T_w > T_{sat,p\_d}$ (Evaporation),

$$\dot{m}_{wv} = c_e \ \ \alpha_w \rho_w \left(\frac{T_w - T_{sat,\hat{p}}}{T_{sat,\hat{p}}} \right) \qquad \text{Lee Model [24]}$$

$$\dot{m}_{wv} = -c_e' \ \ \alpha_w \rho_w \qquad \text{Empirical form} \tag{1}$$

Such that, $T_w \gg T_{sat,\hat{p}}$

$$c_e' = c_e \left(\frac{T_w - T_{sat,\hat{p}}}{T_{sat,\hat{p}}} \right) = \frac{1}{\Delta t}$$

The enthalpy source in energy equation applied for air phase is defined as

$$Q_{va} = -\dot{m}_{wv} \cdot L \tag{2}$$

L is the latent heat due to evaporation at discharge pressure. Such an empirical model also enables the use of constant thermodynamic properties for the water-liquid in the calculations. Four cases were calculated in this study and the corresponding operating conditions are as shown in Table 1.

Table 1. Evaluated CFD cases and resultant delivery temperature at 11.0 bar

	Speed (rpm)	Water (kg/sec)	Remark	Average Discharge Temperature (°C)
Case1	6000	0.018	2x – twice the saturation mass	325
Case2	4500	0.009	Saturation Mass - x	262
Case3	4500	0.045	5x – five times the saturation mass	205
Case4	6000	0.090	10x – ten times the saturation mass	187

Table 2. Fluid properties

Property	**Air**	**Water Liquid**	**Units**
Density	Ideal Gas	997.0	kg m^{-3}
Dynamic Viscosity	1.83e^{-05}	8.889e^{-04}	kg m^{-1} s^{-1}
Thermal Conductivity	2.61e^{-02}	0.6069	Wm^{-1} K^{-1}
Specific heat capacity	1004.4	4181.7	J kg^{-1} K^{-1}

Fluid properties were defined as in Table 2 with air as the primary phase and water-liquid as the secondary phase. Pressure boundary conditions were specified at the suction and discharge. Solver parameters were set at higher stability conditions. SST k-Omega turbulence model was applied. Results from CFD analysis are presented in this section. They reflect a state when full 11.0 bar discharge pressure has been reached in the discharge port and 1-2 cycles of calculation were continued at these operating conditions. The cycle averaged temperature data were collected during the simulation.

3.1. Internal compression chamber pressure

Figure 13 shows the rise of pressure in the compression chamber with main rotor rotation for Case1 at 6000 rpm and 0.018 Kg/sec water mass flow rate condition. Both air and water are at the same pressure inside the chamber. Because of the high under-compression which can be observed by the steep pressure rise at 350º rotor angle, a strong pressure pulse is generated in the discharge port.

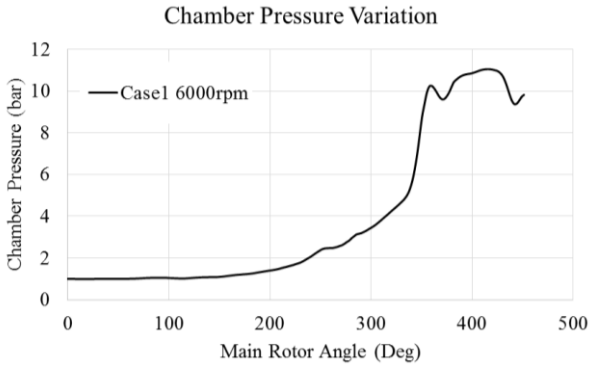

Figure 13. Internal chamber pressure variation during a compression cycle

The indicated power at 6000rpm was 21.0 kW and at 4500rpm it was 15.0 kW. The average torque on the main rotor was close to 30.0 Nm while that on the gate rotor was close to 3.69 Nm. The direction of gate rotor torque was opposite to that of the main rotor. All the four cases have been calculated at 11.0 bar discharge pressure the resultant rotor torque was in the similar range in all the cases.

3.3. Gas temperature distribution

If water was not injected in the compressor, the temperature of air would have exceeded 380°C at 11.0 bar discharge pressure. In the analysed cases, water has been injected at 10°C. Table 1 presents the average air temperature at the discharge in the four cases. It can be observed that for a low water mass flow rate of 0.009 Kg/sec the cooling effect was stronger in Case 2 at 4500 rpm compared to Case 1 at 6000rpm which had twice water mass flow compared to Case 2.

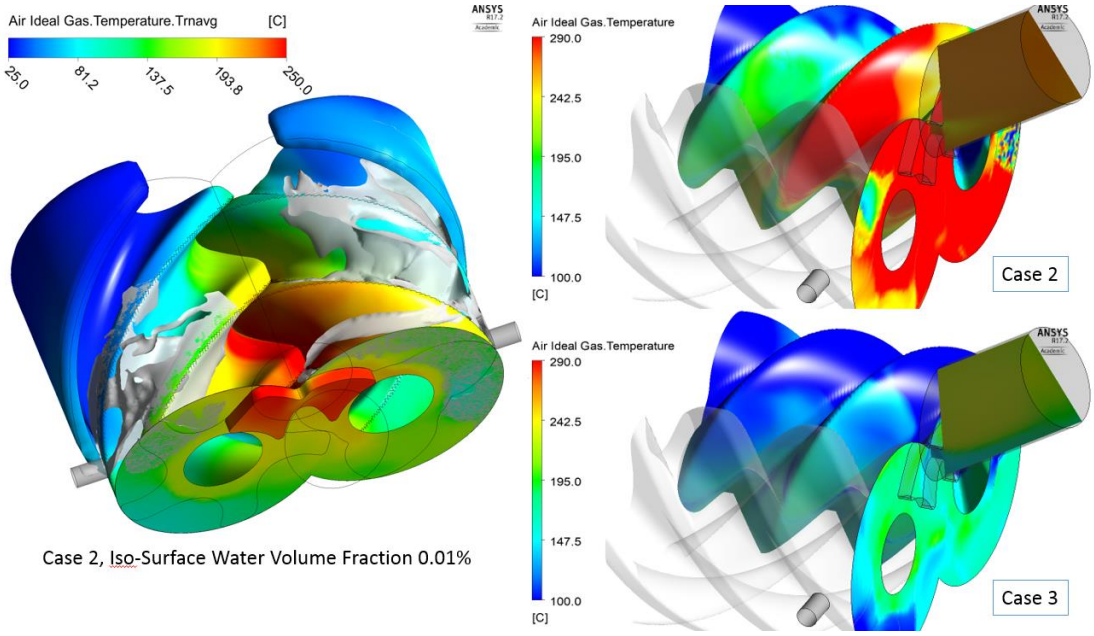

Figure 14. Iso-surface of liquid water and cycle averaged air temperature distribution

The water mass of 0.009 Kg/sec was determined so as to achieve saturated air at the exit with power dissipation of approximately 30 kW. But these estimates did not account for transient affects.

CFD calculation has therefore resulted in higher than saturation exit temperatures. Additionally the leakage of gas during compression adds to the accumulation of energy in the compression chamber which further raises the gas temperature. Cases 2 and 4 were designed such that the mass flow rate of water is 5 times and 10 times that of the saturation mass of Case 2 respectively with the aim of achieving a discharge temperature lower than 200°C. The limit of 200°C is due to the maximum temperature that the compressor bearings and housing can withstand during operation. It can be observed from Table 1 that the temperature of 205°C is achieved at 4500 rpm and 187°C is achieved at 6000rpm with increased mass flow of water. Figure 14 presents the distribution of air temperature inside the compressor. An iso-surface generated with water-liquid volume fraction of 0.01% is also shown in the figure. The temperature in the suction port is lower on the gate rotor side, but on the main rotor side shows higher air temperature. This indicates that the leakage is higher from the tip of the main rotor as compared to the gate rotor and also that the cooling is more effective on the gate rotor side as compared to the main rotors side for the same mass of injected water. The temperature on the gate rotor is higher than on the main rotor close to the discharge port. Water-liquid is observed in the region where air temperature is below the saturation temperature at 11.0 bar. Evaporation effect is visible in the compression chamber opened to the discharge port and also in the discharge port i.e. no liquid water is present here. In comparison to Case 2, Case3 showed about 50°C lower cycle average temperature.

3.2. Evaporation effect

Figure 15 shows the representative water-vapour formation and cooling of air. Figure 15a shows the air temperature distribution on the main rotor surface, in the end leakage and in a plane through the discharge port. Figure 15b shows the region where liquid water is getting converted to vapour. Figure 15c shows the distribution of liquid water on the main rotor surface and Figure 15d shows the latent heat energy being removed from air in regions where evaporation is active.

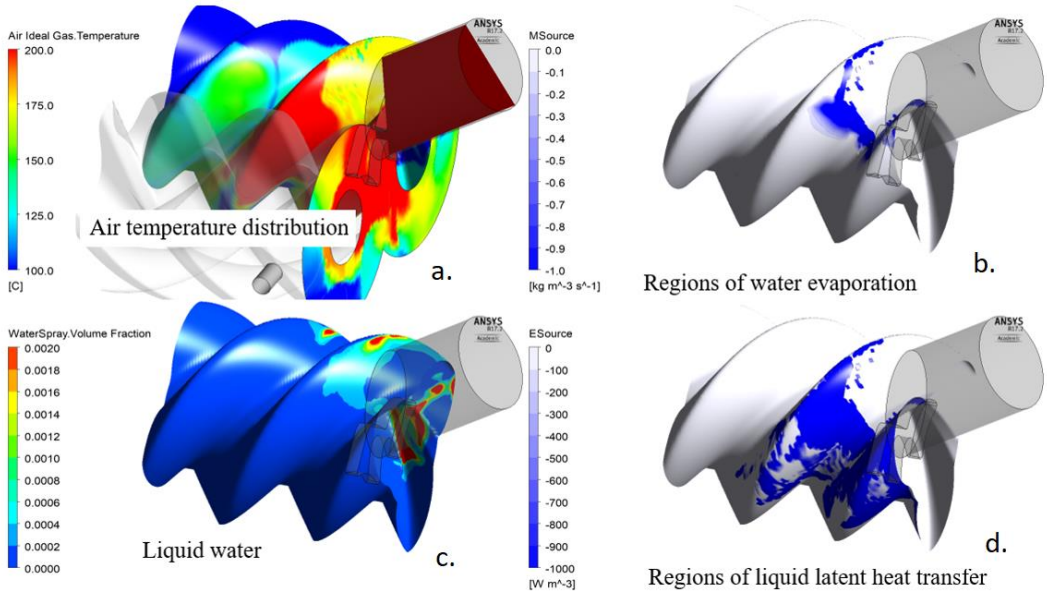

Figure 15. Visualization of Case 2, a) Air temperature distribution, b) Regions of water evaporation, c) Liquid water distribution and d) Regions of liquid latent heat transfer

The air temperature and presence of liquid water can be correlated to the regions of vapour formation and heat extraction in this figure. Due to very low mass of water - 0.009 Kg/sec in the Case 2 the local air temperature reaches to about 290°C. In Case 3 which had 5 times higher mass injection as compared to Case 2 the peak air temperature dropped to below 200°C as shown in Figure 14.

4. Discussion

Rotary screw machines in their current form have been in operation for a long time and the basic design has not changed. Classical twin screw and single screw rotor arrangements have been successfully used as compressors, pumps and expanders. With ever-increasing demands for higher efficiency, operating pressure ratio and reliability, designers are constantly exploring non-conventional rotary arrangements. 3D CFD models are being used more and more to improve rotary machine design by optimizing the rotors, ports and the interaction of flow within the working chambers. The use of 3D CFD for exploring non-conventional design space has been chiefly constrained by the non-availability of computational mesh generation tools. In this paper, SCORG, a customized grid generation tool that has a framework developed for classical twin screw machines has been presented as applied to other variety of screw machines. It was possible to extend the grid generation to a variety of variable geometry rotors such as rotor lead variation or rotor profile variation. Similarly, a completely non-conventional internally geared conical screw machine could be designed. Other arrangements include multiple gate rotors intended to increase volumetric displacement or the dual lead high wrap angle rotors intended for very high-pressure differences. The availability of computational grid for such screw rotors now makes it possible to evaluate the flow and thermal field in the working chambers of these machines.

The test case of water injected twin screw compressor is an example of multi-phase flow consisting of two fluids air and water. A single domain structured numerical mesh of the flow domain was generated using recently developed boundary blocking, analytical grid generation and elliptical smoothing by SCORG. Analysis of the test cases indicate the following design performance:

- Results show higher cooling at 4500 rpm than at 6000 rpm for the same water mass flow rate. Total mass of water injected and its residence time in the compression chamber is higher at lower speed resulting in greater heat transfer and cooling. At 4500 rpm the compression power is lower than at 6000 rpm. Therefore the same mass of water will provide higher cooling at lower speeds.
- When water mass required just for saturation is injected, the exit temperature exceeds 300 C. By injecting five times higher water mass flow, cycle average temperature close to 200 C could be achieved.
- In this compressor design, water cooling effect was higher on the Gate rotor side due to early injection. An increase in the water injection on main rotor side can help to achieve better temperature uniformity.
- Tip leakage is higher on Main rotor side and this results in non-uniform temperature on the housing.

The test case demonstrated that physical mechanism such as injection of water in the compression chamber and evaporation during the compression cycle is still at a primitive level where simplification of the evaporation mechanism was required to avoid excessively high computational resource and facilitate numerical stability of the flow solver. This implies the need to further develop numerical models and flow solvers to be suitable for the design and analysis of rotary screw machines.

5. Conclusion

It is anticipated that more customized grid generation tools such as SCORG will need to be developed as further positive displacement screw machine designs are explored and their computational models are demanded. Additional 3D CFD methods that can provide robust grid re-meshing algorithms or meshless methods will also need to be evolved that can be used for flow computation in complex deforming domains of these machines.

Nomenclature

ALE	Arbitrary Lagrangian Eulerian	Q_{va}	Evaporation enthalpy source
CFD	Computational Fluid Dynamics	$\dot{m}_{wv}$	Evaporation mass source

PDE	Partial Differential Equations	Δt	Solver time step size
TFI	Trans-finite Interpolation	c_e	Lee – Mass transfer coefficient
L	Latent heat	c_e'	Empirical mass transfer coefficient
T_w	Water temperature	$\hat{p}$	Vapour partial pressure
ρ_w	Water density	α_w	Water volume fraction
η_v	Volumetric efficiency	η_a	Adiabatic efficiency
$T_{sat,\hat{p}}$	Saturation temperature at vapour partial pressure	SCORG	Screw Compressor Rotor Grid Generator

Supplementary Materials: The following are available online at http://pdmanalysis.co.uk/gallery/ , Video S1: Variable lead rotors, Video S2: CFD Simulation of Oil Injected Twin Screw Compressor, Video S3: Tri-rotor screw machine, Video S4: SCORG Grid for internal screw rotors.

Author Contributions: conceptualization, S.R., A.K. and N.S.; methodology, S.R. , A.K. and N.S.; investigation, S.R., A.K. and N.S.; writing—original draft preparation, S.R.; writing—review and editing, A.K. and N.S.; supervision, N.S.; project administration, S.R. and A.K.

Funding: This research was funded by the Centre for Compressor Technology, City, University of London.

Acknowledgments: Authors would like to thank Professor Ian K Smith, Centre for Compressor Technology, City, University of London for supporting the research and Mr Graham Stupple and Mr Andreas Korner from Jäcklin GmbH for water injected screw compressor technical inputs.

Conflicts of Interest: The authors declare no conflict of interest.

References

1. Rane, S. Grid Generation and CFD analysis of Variable Geometry Screw Machines, Thesis, City, University of London, **2015**.
2. Gardner, J. W. US Patent No 3,424,373 – Variable Lead Compressor, **1969**.
3. Kovačević, A. Three-Dimensional Numerical Analysis for Flow Prediction in Positive Displacement Screw Machines, Thesis, City, University of London, **2002**.
4. Kovačević, A. Boundary Adaptation in Grid Generation for CFD Analysis of Screw Compressors, Int. J. Numer. Methods Eng., **2005**, Vol. 64: 401-426.
5. Stošić, N.; Smith, I.K.; Kovačević, A. Screw Compressors: Mathematical Modeling and Performance Calculation, Monograph, Springer Verlag, Berlin, **2005**, ISBN: 3-540-24275-9.
6. Kovačević, A.; Stošić, N.; Smith, I. K. Screw compressors - Three dimensional computational fluid dynamics and solid fluid interaction, **2007**, ISBN 3-540-36302-5, Springer-Verlag Berlin Heidelberg New York.
7. Sauls, J.; Branch, S. Use of CFD to develop improved one-dimensional thermodynamic analysis of refrigerant screw compressors. 8th Int conf on compressors and their systems, **2013**, p. 591.
8. Mujic, E. A Numerical and Experimental Investigation of Pulsation Induced Noise in Screw Compressors, PhD Thesis, London: City University of London, **2008**.
9. Riemslagh, K.; Vierendeels, J.; Dick, E. An arbitrary Lagrangian-Eulerian finite-volume method for the simulation of rotary displacement pump flow. Applied Numerical Mathematics, **2000**, 32:419-433.
10. Voorde Vande, J.; Vierendeels, J. A grid manipulation algorithm for ALE calculations in screw compressors. 17th AIAA Computational Fluid Dynamics Conference, Canada, **2005**, AIAA 2005-4701.
11. Rane, S,; Kovačević A. Algebraic generation of single domain computational grid for twin screw machines. Part I. Implementation, Advances in Engineering Software, **2017**, 107, pp. 38-50, doi: 10.1016/j.advengsoft.2017.02.003
12. Kovačević, A.; Rane, S. Algebraic generation of single domain computational grid for twin screw machines Part II – Validation, Advances in Engineering Software, **2017**, 107, pp. 31-43, doi: 10.1016/j.advengsoft.2017.03.001
13. Schulze-Beckinghausen, P.; Hauser, J.; Beinert, M.; Herlemann, S. Advanced analysis of twin screw compressors with variable rotor pitch using one-dimensional thermodynamic simulation, International screw compressor conference, TU Dortmund, VDI-Berichte, **2014**, 2228 ; 237-248 .
14. Utri, M.; Brümmer, A. A comparative examination of the potential of screw expanders with variable rotor pitch, International screw compressor conference, TU Dortmund, VDI-Berichte, **2014**, 2228 ; 249-266.

15. Kauder, K.; Fost, C. Investigations about the improvement of the Filling process of a Screw–Type Engine, Part III. VDI-Berichte Report, TU Dortmund, **2002**.
16. Fost, C. Geometrical Variations at the Inlet of Screw–Type Engines. International screw compressor conference, VDI-Berichte Nr. 1932, TU Dortmund, **2006**.
17. Rane, S.; Kovačević, A.; Stošić, N.; Kethidi, M. Grid Deformation Strategies for CFD Analysis of Screw Compressors, Int Journal of Refrigeration, **2013**, 36, 7, p. 1883-1893.
18. Rane, S.; Kovačević, A.; Stošić, N.; Kethidi, M. Deforming grid generation and CFD analysis of variable geometry screw compressors, Computers and Fluids, **2014**, 99, p. 124–141.
19. Knupp, P.; Steinberg, S. The Fundamentals of Grid Generation. ISBN 9780849389870, **2002**, CRC Press.
20. Rane, S.; Kovačević, A. Application of numerical grid generation for improved CFD analysis of multiphase screw machines, 10th *International conference on compressors and their systems*, London, IOP Conf. Ser.: Mater. Sci. Eng., **2017**, **232,** 01. doi.org/10.1088/1757-899X/232/1/012017
21. Crowe, T. C. Multiphase Flow Handbook. Taylor and Francis, **2006**, ISBN 0-8493-1280-9, CRC Press.
22. Rane, S., Kovačević, A.; Stošić, N. CFD Analysis of Oil Flooded Twin Screw Compressors. Int. Compressor Eng. Conference, Purdue, **2016**, Paper 2392.
23. Nilsson, H. R. US Patent No 2,481,527 – Rotary Multiple Helical Rotor Machine, **1949**.
24. Rane, S.; Kovačević, A.; Stošić, N.; Stupple, G. On Numerical Investigation of Water Injection to Screw Compressors. ASME. ASME International Mechanical Engineering Congress and Exposition, Volume 6A: Energy:V06AT08A031, **2019**, doi:10.1115/IMECE2018-86463.